

Proceedings of the Eurosensors XXIII conference

# Swarm Absolute Scalar and Vector Magnetometer Based on Helium 4 Optical Pumping

Jean-Michel Leger<sup>(a)\*</sup>, François Bertrand<sup>(a)</sup>, Thomas Jager<sup>(a)</sup>, Matthieu Le Prado<sup>(a)</sup>,  
Isabelle Fratter<sup>(b)</sup>, Jean-Claude Lalaurie<sup>(b)</sup>

<sup>a</sup>CEA, LETI, MINATEC, F38054 Grenoble, France

<sup>b</sup>Centre National d'Etudes Spatiales, 18 Avenue Edouard Belin, 31401 Toulouse Cedex 9, France

---

## Abstract

The CEA-LETI has successfully designed and realized an optically pumped <sup>4</sup>He magnetometer which provides absolute scalar magnetic field measurements with a 1 pT/√Hz resolution over a DC to 100 Hz bandwidth. Its final corrected scalar accuracy has been demonstrated to be better than 50 pT. The ASM instrument is also able to provide vector field measurements with an intrinsic 1 nT/√Hz resolution and a 0.4 Hz bandwidth. All ASM components have now been successfully qualified with respect to the environment and performances specifications of the SWARM mission and the different ASM flight models are currently being manufactured and will be available for the SWARM satellites integration in 2010.

*Keywords:* scalar magnetometer ; vector magnetometer ; <sup>4</sup>He optical pumping ; high resolution magnetometer

---

## 1. Introduction

The Absolute Scalar Magnetometer (ASM) developed by CEA-LETI in partnership with CNES is an optically pumped <sup>4</sup>He magnetometer which shall provide absolute scalar measurements of the magnetic field with high accuracy and stability for the calibration of the Vector Field Magnetometer (VFM) developed by the Danish National Space Center. These magnetometers will be flown on each of the 3 satellites of the SWARM mission, dedicated to carry out the best ever survey of the Earth magnetic field. In addition and on an experimental basis the ASM will be able to operate as a vector field magnetometer. Both operating principle and related performances are detailed in the following paragraphs.

## 2. ASM operating principle

The ASM is an optically pumped <sup>4</sup>He magnetometer based on an electronic magnetic resonance whose effects are amplified by a laser pumping process [1,2], as detailed on Fig. 1. A fraction of the atoms of a <sup>4</sup>He gaz cell are first excited to the 2<sup>3</sup>S<sub>1</sub> metastable state by means of a high frequency discharge. This energy level is split by the static

---

\* Corresponding author. Tel.: +33 0 04 38 78 48 16; fax: +33 04 38 78 51 59.

E-mail address: [jean-michel.leger@cea.fr](mailto:jean-michel.leger@cea.fr).

magnetic field  $B_0$  into three Zeeman sublevels. As the energy gap  $\Delta E$  between the levels is directly proportional to the ambient scalar field  $B_0$ , its determination allows the measurement of  $B_0$  (1).

$$\Delta E = \gamma \hbar B_0 \quad \text{where } \gamma \text{ is the } ^4\text{He gyromagnetic ratio for the } 2^3\text{S}_1 \text{ state [3]} \quad (1)$$

The measurement of  $B_0$  is then performed by exciting and detecting the paramagnetic resonance between the Zeeman sublevels. To generate the resonance an oscillating radiofrequency field  $B_1$  is applied on the  $^4\text{He}$  gaz cell: when its frequency matches the Larmor frequency of the Zeeman sublevels ( $\omega_0 = \gamma B_0$ ) the magnetic resonance occurs and transitions are induced between the sublevels.

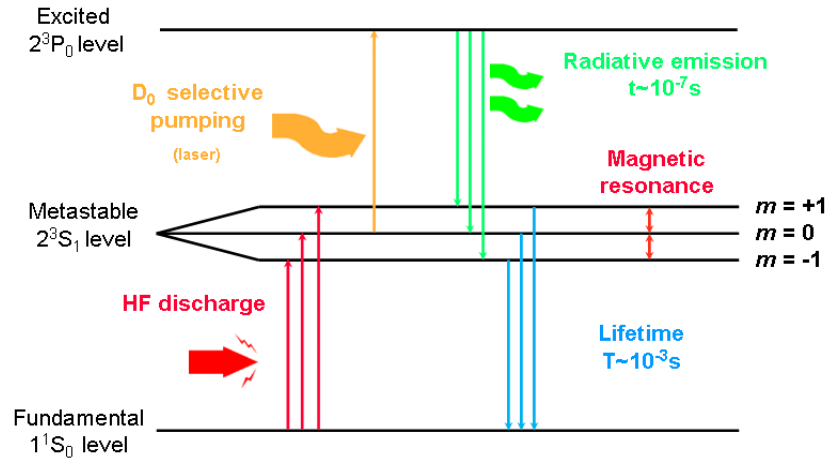


Fig. 1.  $^4\text{He}$  energy diagram and ASM principle of operation

However, at thermal equilibrium the sublevels are almost equally populated and no significant change induced by the resonance can be detected. To finally enhance and detect the resonance, a selective pumping from one of the Zeeman sublevel to the  $2^3\text{P}_0$  state is performed thanks to a frequency tuned linearly polarized laser light. The resulting disequilibrium between the Zeeman sublevels populations improves the resonance signal amplitude by several orders of magnitude while the monitoring of the intensity of the laser light transmitted through the  $^4\text{He}$  cell allows its detection.

The ASM magnetometer can also provide a vector measurement of the magnetic field using the information provided by the superimposition of 3 low pulsation orthogonal magnetic fields onto the  $B_0$  field seen by the  $^4\text{He}$  sensing cell (2).

$$\|\vec{B}_{tot}\| = \left\| \vec{B}_0 + \sum_{j=1}^3 \beta^j \cos(\omega_j t) \vec{e}_j \right\| \quad (2)$$

The vector measurement is simply obtained by processing the scalar output measurement containing the principal harmonics at the  $\omega_j$  pulsations. The vector field reconstruction in the ASM reference frame is finally achieved thanks to a specific calibration process [2] where the vector modulation amplitudes  $\beta_j$  and their respective orientations  $\vec{e}_j$  in the ASM frame are derived.

### 3. ASM hardware architecture

To take full advantage of the scalar magnetometer performances we have defined an architecture that is free of the orientation effects common to all standard scalar magnetometers based on magnetic resonance. The final

instrument assembly consists of an electronic box (Digital Processing Unit) and a separately installed sensor connected to the electronic box by a bundle of optical fibers and electrical cables (harness). As cold redundancy has been required for the instrument, a specific sensor bracket has been designed to mechanically interface two identical sensors at the tip of the satellite boom, each sensor being connected to a dedicated DPU located within the satellite main body.

Since this CEA-LETI magnetometer technology will be launched and operated in space for the first time, all ASM elements have been validated with respect to the environment specifications of the mission. A number of ASM specific and complex components such as the fiber Bragg grating laser have been successfully developed and qualified. A picture of the final ASM components including the ASM sensor assembly, the ASM DPU and the optical and electrical harnesses is given in Fig. 2(a). The different ASM flight models are currently being manufactured and will be available for the SWARM satellites integration in 2010.

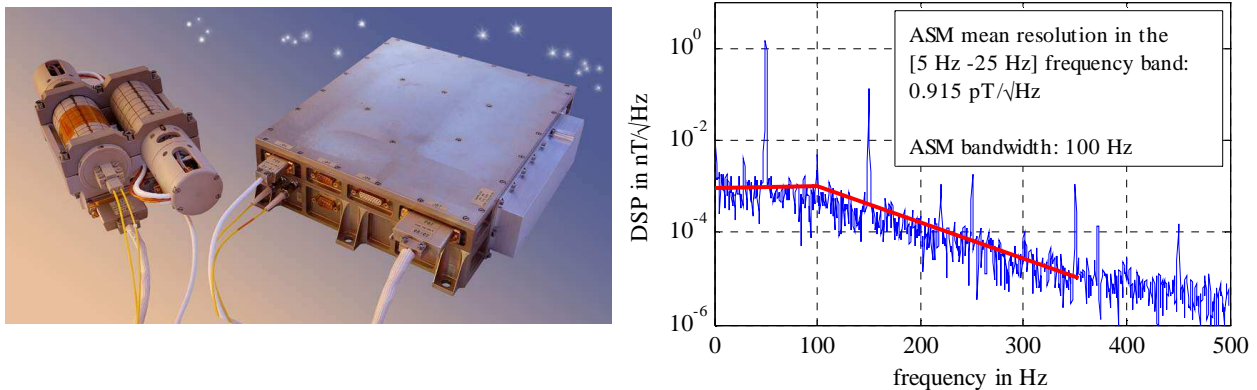


Fig. 2. (a) ASM sensor assembly and ASM DPU; (b) ASM scalar bandwidth and resolution

#### 4. ASM performances

Compared to the Overhauser based scalar sensors previously used for the Ørsted and CHAMP missions [4], the scalar resolution has been enhanced to  $1 \text{ pT}/\sqrt{\text{Hz}}$  and the scalar bandwidth previously limited to few Hz can be increased up to 300 Hz. For the SWARM mission, the scalar bandwidth has been set to 100 Hz so that vector modulations frequencies can be adjusted over a large band of frequencies below 50 Hz. The ASM scalar bandwidth and resolution are illustrated on Fig. 2(b).

The following specific errors affecting the scalar magnetic field measurement have been identified and characterized: the ASM sensor anisotropy, the vector modulations aliasing, the Bloch-Siegert effect [5], the measurement datation error and the Pulse Per Second (PPS) time reference accuracy. The measured and calculated maximum contributions are given in Table 1. Corresponding maximum remaining errors after the ASM level 1B algorithms corrections are also given and a resulting quadratic residual error on the absolute accuracy of about 50 pT is demonstrated. Additional error contributions such as the satellite magnetic moment and the magnetocouplers effect will be corrected at satellite level with the SWARM satellite level 1B algorithms.

Table 1. ASM errors contributions on the scalar measurement (residual quadratic error after level 1b corrections:  $\sigma_{\text{max}} = 50 \text{ pT}$ )

Error type	Bloch-Siegert error	Vector aliasing	ASM in-orbit anisotropy	PPS precision ( $5 \cdot 10^{-7} \times B_0$ ) (worts case)	Datation (1 ms x 30 nT/s) (worst case)
Initial uncorrected ASM error	55 pT (@ 46 $\mu\text{T}$ )	23 pT (@ 46 $\mu\text{T}$ )	120 pT	32,5 pT (@ 65 $\mu\text{T}$ )	30 pT
Remaining error after ASM	< 5 pT	< 5 pT	< 25 pT	32,5 pT (@ 65 $\mu\text{T}$ )	30 pT

level 1B algorithm correction

(system error, not corrected in the level 1B algorithms) (instrument error, not corrected at level 1B)

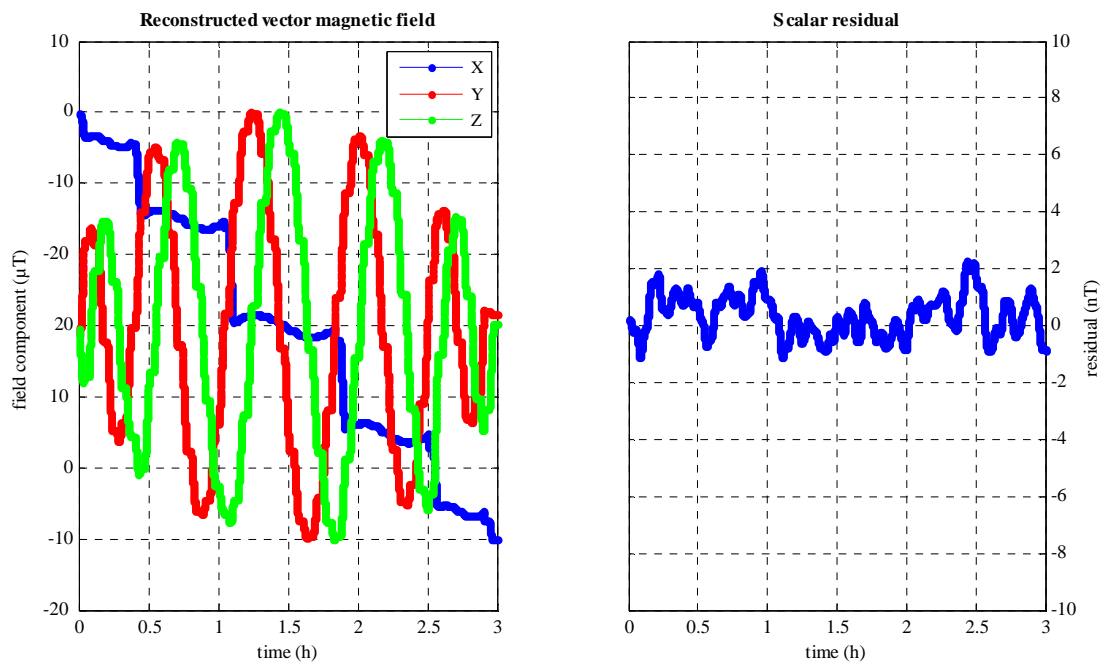


Fig. 3. (a) ASM vector calibration magnetic figure : 15  $\mu\text{T}$  modulus spiral ; (b) corresponding scalar residual

While the main objective of the ASM is to provide high resolution scalar measurements for the calibration of the VFM sensor, the ASM is also able to provide absolute vector measurements. Its vector resolution is in the  $\text{nT}/\sqrt{\text{Hz}}$  range [2] for a vector measurement bandwidth set to 0.4 Hz and an accuracy of about 1 nT. To be properly used, the vector mode has to pass a calibration process detailed in [2], and derived calibration parameters will be used in the ASM vector level 1B algorithm. This process is illustrated on Fig. 3(a) and on Fig. 3(b) corresponding to the measurements taken during a 3D calibration spiral applied on the ASM sensor, resulting in a preliminary scalar residual lower than  $\pm 2$  nT peak-to-peak.

## References

1. Colegrove, F. D. and L. D. Scheerer, "Optical pumping of helium in the  $3S_1$  metastable state", *Physical Review*, 119, 680–690, 1961.
2. O. Gravrand, A. Khokhlov, J.L. Le Mouél, and J. M. Léger, "On the calibration of a vectorial  $4\text{He}$  pumped magnetometer," *Earth Planets Space*, 53, 2001, p. 949–958.
3. Shifrin V.Y. and al," Experimental Determination of the Gyromagnetic Ratio of the Helium-4 Atom in Terms of that of the Helium-3 Nucleus", *IEEE Transactions on Instrumentation and Measurement*, Vol.46, No. 2, 1997, p. 97-100.
4. D. Duret, J.M. Léger, M. Francès, J.Bonzom and F. Alcouffe, "Performances of the OVH Magnetometer For The Danish Oersted Satellite", *IEEE Transactions On Magnetics*, Vol. 32, No. 5, 1996, p. 4935-4937.
5. J.A. Hermann and S. Swain, "Bloch-Siegert shifts and multi-quantum transitions in spin-one systems", *J. Phys. B: Atom. Molec. Phys.*, Vol 10, No. 11, 1977, p. 2111-2123.